

Peak resistance temperature and low temperature resistivity in thin $\text{La}_{1-x}\text{Ca}_x\text{MnO}_3$ mixtures for $x = 1/3$

P. R. Broussard

Covenant College, Lookout Mountain, GA 30750

Abstract

The electrical resistivity of $\text{La}_{1-x}\text{Ca}_x\text{MnO}_3$ thin films grown on (001) NdGaO_3 and (100) SrTiO_3 substrates by o -axis sputtering has been studied as a function of the Calcium doping level. The samples have very narrow rocking curves and excellent in plane registry with the substrate. A strong correlation between the peak resistance temperature and the polaronic hopping energy is seen which is not simply linear. The low temperature resistivity is seen to be better by a model of single magnon scattering, and a near linear correlation between the resistivity due to magnon scattering and static impurities is observed.

PACS numbers: 75.47.Lx, 75.47.Gk, 73.50.-h, 75.50.-y, 81.05.Je

I. INTRODUCTION

The discovery of colossal magnetoresistance (CMR) in the doped manganite materials¹ and subsequent study of the properties of these materials has created a great deal of interest in both the application and the underlying cause of CMR. The connection between the Double Exchange mechanism and the Jahn-Teller lattice distortions has focused attention on the carriers in the systems. Much work has been done to show that the adiabatic small polaronic model fits the resistivity above the metal-insulator (MI) transition in the $\text{La}_{1-x}\text{Ca}_x\text{MnO}_3$ (LCMO) system.^{2,3,4} In an earlier publication,⁵ the anomalous behavior of the peak resistance temperature for $\text{La}_{1-x}\text{Ca}_x\text{MnO}_3$ films with x varying from 0 to 1/3 was mentioned, where the temperature for the metal-insulator transition (T_{MI}) or the peak resistance temperature (T_p) was higher than that seen in bulk materials for $x < 0.25$ and that the metal-insulator transition persisted below the $x = 0.175$ value which is the boundary in bulk materials for this transition. Similar results were seen in the work by Prellier et al.⁶ for films of $\text{La}_x\text{Ca}_{1-x}\text{MnO}_3$ for $0.1 < x < 0.5$ grown on LaAlO_3 . Recent work on LCMO material has addressed the connection between the polaronic hopping energy and the peak resistance temperature³, as well as the behavior of the low temperature resistivity in the manganites.⁷ In this paper, the films studied in the earlier work⁵ are examined in light of these recent analysis. In particular, it is shown that 1) there is a definite relationship between the polaronic hopping energy and the peak resistance temperature, but the relationship is more complicated than Song et al. found, and 2) the low temperature behavior of the resistivity is more consistent with the model by Jaime et al.⁸

II. SAMPLE PREPARATION AND CHARACTERIZATION

The samples were grown by *o*-axis sputtering using composite targets of $\text{La}_{0.67}\text{Ca}_{0.33}\text{MnO}_3$ (LCMO) and LaMnO_3 (LMO) material mounted in copper cups. The substrates were (001) oriented neodymium gallate (NdGaO_3) and (100) oriented strontium titanate (SrTiO_3), silver-pasted onto a stainless steel substrate holder that was radiatively heated from behind by quartz lamps. Although there was no direct measurement of the holder temperature for the runs used in this study, previous runs (under nominally the same conditions) using a thermocouple clamped onto the front surface of the holder indicated a

temperature of 670 °C. The LMO target was radio frequency sputtered and the LCMO target was direct current sputtered in a sputter gas composed of 80% Ar and 20% O₂ (as measured by flow meters) and at a total pressure of 13.3 Pa. These conditions gave deposition rates of 17-50 nm/hr, with film thicknesses being typically 150-300 nm. After deposition, the samples were cooled in 13.3 kPa of oxygen. From previous work⁹ it is known that this process can grow manganite films that have low resistivities and high peak temperatures without the use of an ex-situ anneal in oxygen.

The Ca concentration in the films, x , was determined by X-ray fluorescence measurements, which in turn were calibrated by Rutherford Backscattering (RBS) for companion samples deposited on MgO substrates. The samples were characterized by standard and high resolution x-ray diffraction scans (using a Philips MRD x-ray diffraction system, with a four-crystal Ge 220 monochromator on the incident beam and CuK_{α1} radiation ($\lambda = 1.5045$ Å)). 2 θ scans were taken both along and at various angles to the growth direction, as well as rocking curves and ω scans (where 2θ is set for a particular reflection at an angle to the film normal, and the film is rotated about the film normal) to look for misoriented grains. Electrical resistivity measurements were made using the van der Pauw method¹⁰.

III. STRUCTURE OF THE FILMS

X-ray diffraction shows that the films on both substrates are oriented (00L) (orthorhombic notation) perpendicular to the film plane. Fig. 1 compares the x-ray diffraction scans taken in standard resolution mode (Cu K_α radiation) for a film with $x=0.18$ on SrTiO₃ and NdGaO₃. The reduction in the c-axis lattice constant induced by the film attempting to lattice match to the larger lattice constant of SrTiO₃ and the opposite for the case on NdGaO₃ is clearly seen. The c-axis lattice constant increases as the Ca concentration is decreased, similar to that seen in bulk material.¹¹ The samples on NdGaO₃ show more strain for low values of x while the samples on SrTiO₃ have more strain near $x = 1/3$. The samples on NdGaO₃ are on average more strained than samples on SrTiO₃ are for intermediate values of x .

The film quality for the samples on NdGaO₃ is excellent, with rocking curve widths for the (004) reflection of the order of 200 arc-seconds (with an instrumental resolution of 15 arc-seconds). The films on SrTiO₃ had broader rocking curve widths, typically of order

300 arc-seconds, partly due to the fact that the SrTiO_3 substrates have large rocking curve widths since they are grown by a flame fusion process, rather than the Czochralski method used for NdGaO_3 substrates. The in-plane order for the MnS , however was similar between the two substrates. Fig. 2 shows a phi-scan for the (022) reflections for both NdGaO_3 and LaMnO_3 for the $x = 0$ sample grown on NdGaO_3 and a similar plot for the $x = 1/3$ sample grown on SrTiO_3 . Excellent registry between the MnS and the substrate is seen in both cases. (The reason for the 4-fold rather than the expected 2-fold symmetry for both materials is due to the acceptance angle on the detector seeing both the (202) and (022) reflections.) The rocking curve widths for the (022) LCMO reflections are similar to those seen for the (004) reflections.

IV. PEAK TEMPERATURE AND RESISTIVITY

Fig. 3 shows the resistivity vs. temperature for several of the as-deposited MnS , which have low resistivities and high peak transition temperatures (T_p). Typically, the MnS on SrTiO_3 have values of T_p that are 15 K lower than MnS on NdGaO_3 , as well as higher resistivities, even though the MnS on NdGaO_3 are under more strain usually. For samples with $x = 1/3$, the resistivity at low temperatures is less than $0.4 \text{ m}\Omega\text{-cm}$, and show a greater than two order of magnitude reduction from the resistivity at T_p , both of which have been used as measures of MnS quality.^{3,7} As was noted in the earlier work⁵, the samples on both substrates maintain a high value of T_p even for low values of x . This report now turns to two areas of the resistivity of the samples.

A. T_p and high temperature resistivity

Much work has been done to understand the interaction between the Double Exchange model and the CMR effect in these materials. Presently the connection is made that polaron interactions are responsible for the CMR effect, which implies that above the peak temperature the resistivity should be dominated by the adiabatic small polaronic resistivity, which is given by $\rho(T) / T \exp \frac{E_{\text{hop}}}{k_B T}$. For the temperature range considered in this study, both the small polaron model as well as the Arrhenius relation $\rho(T) / \exp \frac{E_a}{k_B T}$ fit the data equally well. In the work by Song et al.³, they found a correlation between the activation energy,

E_{hop} , and the value of T_p for oxygen deficient LCMO films, which they interpreted as a linear dependence. For the films in this study, Fig. 4 presents a similar study, including results for films of this study that were subsequently annealed to 700 °C in oxygen, which resulted in an increase in their peak temperature. Clearly in this case the dependence between T_p and E_{hop} is not linear over the whole range, although there is direct relationship between the two. This dependence is very similar to what was observed by Browning et al.¹³ where they found a correlation between the activation energy (assuming a simple Arrhenius relation) and the Curie temperature of radiation damaged LCMO films. One can see that over a limited range of this plot, a linear relationship could be found, but clearly the whole range is more complicated. In fact the plot seems to show that as the polaronic hopping energy gets large enough, the metal-insulator transition is more rapidly depressed. What is interesting is that the values here are similar to those found by Song et al. even though their values are for a fixed cation composition and varying oxygen contents, while the films here are for varying dopant levels. The plot also presents results for LCMO films produced in a similar manner as the films here but on different substrates or growth temperatures. These are labeled as "LCMO" on the plot. Clearly there seems to be a behavior that is more universal than just for carefully controlled samples.

B. Low temperature resistivity

Several attempts have been made to describe the low temperature behavior of the resistivity for the manganate materials. In an attempt to explain data which implies a $T^{2.5}$ dependence, such as seen in Schi er et al.¹², Wang and Zhang¹⁴ have looked at the system with single magnon scattering and where the minority spin states near the Fermi edge are Anderson localized. They predict that the resistivity will go as $T^{2.5}$ until the temperature decreases below 60K, when the behavior changes to $T^{1.5}$. Recently, Mercone et al.⁷ saw the resistivity of LCMO and LSMO films grown by various techniques behaving as $T^{2.5}$ with $T^{2.5}$ for the low temperature range. Jaime et al.⁸ have also looked at the case of single magnon scattering, but in their case the minority carriers are not localized. In this model, the single magnon scattering term will go as T^2 , but with a temperature dependent coefficient that is due to an energy shift between the minority and majority spin bands. The signature of this type of behavior is a strong reduction in the T^2 term as the temperature is

decreased below the minimum magnon energy that would allow scattering between the spin up and down energy bands.

As observed in earlier work⁹ and is observed here, the low temperature resistivity for these films is better fit by

$$\rho(T) = \rho_0 + \rho_2 T^2 + \rho_5 T^5: \quad (1)$$

The present data was examined to see if it can be explained by the work of Wang and Zhang, especially with the predicted change in temperature dependence, to no avail. What is found is that, as was seen in Jaime et al., there is a reduction in the T^2 term, typically below 30K. As such, the low temperature resistivity data for the films was fit using Eq.1 modified by the model of Jaime et al. The equation used is

$$\rho(T) = \rho_0 + \frac{\rho_2}{2=6} T^2 \int_{T_q=T}^{\infty} \frac{x^2}{\sinh^2(x)} dx + \rho_5 T^5 \quad (2)$$

where T_q represents the term $D \epsilon_{\text{min}}^2 = 2k_B$ in Jaime et al., with $D \epsilon_{\text{min}}^2$ being the minimum magnon energy that would allow scattering between the spin up and down energy bands. ρ_2 represents the single magnon scattering contribution to the resistivity in the absence of any energy gap. The fit also incorporates a static impurity term, ρ_0 , and an electron-phonon term, ρ_5 . The data for $T < T_p=2$ was fit using the simplex minimization routine of Nelder and Mead,¹⁵ which minimizes an average weighted chi squared,

$$\chi^2_W = N = \frac{1}{N} \sum_{i=1}^N \frac{(\rho_{\text{fit}}(i) - \rho_{\text{exp}}(i))^2}{\rho_{\text{exp}}^2(i)} \quad (3)$$

where N is the number of fit points (typically 400). The program would rerun the minimization 5 times from random locations in $(\rho_0; \rho_2; T_q; \text{ and } \rho_5)$ space to ensure the "best" minimization had been found. Typical values of $\chi^2_W = N$ (which is a measure of the rms error per point for the fit) were $2-3 \times 10^3$. The lowest temperature used in the fitting was down to our lowest measured value (6 K or lower), unlike the work by Mercone et al., who had to limit it to 20 K and higher due to upturns in the resistivity. Attempts to use a dependence like $\rho(T) = \rho_0 + AT$ for the films gave values of $\chi^2_W = N$ larger by a factor of 10 than those of Eq. 2. The results of this fitting are shown in Tables I and II. The only films that were not fit were the ones on SrTiO₃ which showed resistivity upturns at low temperatures, which happened for $x < 0.2$.

In Fig. 5 the results of fitting Eq. 2 to the experimental data for the $x = 0.18$ and $x = 1.3$ samples on both SrTiO₃ and NdGaO₃ substrates are shown. The fit quality is

seen to be very good over the entire temperature range. To compare between the proposed models to describe the low temperature behavior, in Fig. 6 the $T < 50$ K data for the $x = 0.2$ sample on NdGaO_3 is shown, along with the results of fitting Eq. 2, along with results of fitting Eq. 1 as well as the T behavior seen by Mercone et al. One can clearly see the T model cannot reproduce the lowest temperature behavior. One can also see that at the lowest temperature, the fit from Eq. 1 underestimates the data, which is due to the suppression of the T^2 term predicted by Jaime et al.

For the films studied here, we see that, in general, there is an increase in ρ_0 and ρ_2 and a decrease in T_q as the Ca concentration decreases. The magnitude of ρ_5 is roughly constant as x is varied, with all the values being higher for films on SrTiO_3 (except for T_q). The value of ρ_5 found here is in the same range, but higher, than found by Jaime et al.⁸, who saw a value around $1 \text{ f-}\Omega/\text{K}^5$. Our values of all our quantities are larger than seen in the LSMO/LCMO composite mixtures⁹ that were derived using Eq. 1. The increase in ρ_0 as x decreases could be tied to the increase in strain for the samples on NdGaO_3 , but that would not hold for the films on SrTiO_3 , which showed a decrease in strain as x decreases. In addition, the fact that the values for ρ_0 being higher on films grown on SrTiO_3 (which had overall lower strain than the films on NdGaO_3) would imply that strain is not the dominant contributor to ρ_0 . The increased rocking curve width for samples grown on SrTiO_3 would imply an increased static disorder due to grain misalignment, which could explain the higher values of ρ_0 . Since the spin wave stiffness, D , has been seen to be a consistent value across different materials with various doping levels ($\sim 170 \text{ meV}\cdot\text{\AA}^2$),^{16,17} a decrease in T_q would imply a reduction in q_{min} , the shift in the Fermi momentum between the minority and majority spin bands as the doping decreases. From Jaime et al. the ρ_2 term is given by

$$\rho_2 = \frac{3}{16} \frac{N J^5}{e^2 E_F^4 k_F} \left(\frac{k_B}{m D} \right)^2 \quad (4)$$

where $N J$ is the electron-magnon coupling energy and E_F , k_F , and m are the Fermi energy, Fermi wavevector, and effective mass for the carriers. It is expected that as x decreases, there will be a reduction in both the values of Fermi wavevector and energy, which would tend to increase the value of ρ_2 . D might be considered to be constant as discussed above. However, without knowing how $N J$ and m vary with x , it will be difficult to draw any firm conclusions.

In the earlier work on LSMO/LCMO composite mixtures,⁹ a correlation was seen between

the magnitude of the T^2 coefficient and the residual resistivity in the $\ln s$. In this work the same correlation is observed, as shown in Fig. 7. This plot shows the relationship between ρ_2 and ρ_0 for the $\ln s$ of this study, along with the $\ln s$ from work on LCMO/LSMO composites⁹, as well as the results reported by Jaime et al.⁸ on $\text{La}_{0.66}\text{Pb}_{0.67}\text{Ca}_{0.33}\text{MnO}_3$ single crystals as well as work by Snyder et al.¹⁸ on LCMO $\ln s$. There is a clear linear correlation between these two values, as was seen before. In the work on LCMO/LSMO composites, the limited data gave an approximate ratio of $60\text{--}70 \times 10^{-6} \text{ K}^{-2}$, while with the more extensive data here the ratio between the two is more of the order of $120 \times 10^{-6} \text{ K}^{-2}$. The interesting thing is that this correlation is seen not only for LCMO $\ln s$ of varying doping, but is also present in mixtures of LCMO and LSMO as well as crystals of Pb doped LCMO. The question arises as to the possible connection between the static resistivity and the amount of single magnon scattering. The work by Snyder et al. showed a similar behavior for their $\ln s$, but the point of this paper is that this correlation holds over a wide range of $\ln s$ as well as values of ρ_0 . For the $\ln s$ of this study, the variation is both due to changes in doping level as well as differing amounts of strain in the samples, which decreases for samples on NdGaO_3 and increases for those on SrTiO_3 as the doping increases. As discussed above, in the model of Jaime et al. the ρ_2 term depends on the carrier concentration in the materials, as well as the electron-magnon coupling, the effective mass of the carriers, and the spin wave stiffness. It is possible to imagine that if strain in the $\ln s$ is one cause of increasing ρ_0 , then there could also be a connection to the scattering of the carriers on spin waves as strain could impact other properties in the expression for ρ_2 . However, it does not appear that strain in the $\ln s$ is the major cause of ρ_0 , and it would be hard to imagine how say an increase in lattice defects would necessarily increase the effectiveness of magnon scattering. The question remains as to whether this correlation is wider than presented here as well as what could be causing the connection between these two scattering processes.

V. CONCLUSION

This work has shown that $\ln s$ of $\text{La}_x\text{Ca}_x\text{MnO}_3$ grown on NdGaO_3 and SrTiO_3 have excellent structural properties, high values of peak resistance temperatures, and low residual resistivities. As seen in the work by Song et al. there is a correlation between the peak

resistance temperature and the polaronic hopping energy, but the correlation is not simply linear, but is more complicated, with a more pronounced reduction in the value of T_p with increased values of E_{hop} . The low temperature resistivity of the samples is not fit well by the model of Merone et al., but is better fit by the model of Jaime et al. which includes a cutoff in the single magnon scattering. There is a strong linear correlation between the static resistivity and the magnitude of the magnon scattering term that is seen to be present in a wide range of films of various types and conditions.

VI. ACKNOWLEDGMENTS

The author would like to gratefully acknowledge the assistance of David Knies for the RBS measurements, as well as Victor Cestone and Andrew Patton in the production and characterization of the films. Some of this work was carried out at the Naval Research Lab under funding from the Office of Naval Research.

-
- ¹ R . von Hel m olt, J . W ecker, B . H olzapfel, L . Schultz, and K . Sam wer, Phys. Rev. Lett. 71, 2331 (1993).
 - ² D . C . W orledge, L M ieve, and T . H . G eballe, Phys. Rev. B 57, 15267 (1998).
 - ³ X . F . Song, G . J . L ian, and G . C . X iong, Phys. Rev. B 71, 214427 (2005).
 - ⁴ Ch . Hartinger, F . M ayr, A . Loidl, and T . K opp, Phys. Rev. B 73, 24408 (2006).
 - ⁵ P R . Broussard and V C . Cestone, M at. Res. Soc. Symp. Proc. 574, 181 (1999).
 - ⁶ W . P rellier, M . R ajeswari, T . Venkatesan, and R . L . G reene, Appl. Phys. Lett. 75, 1446 (1999).
 - ⁷ S . M ercone, C A . Perroni, V . Cataudella, C . Adam o, M . Angeloni, C . A ruta, G . D eFilippis, F . M illetto, A . O ropallo, P . Perna, Y . Petrov, U . S . diUccio, and L . M aritato, Phys. Rev. B 71, 64415 (2005).
 - ⁸ M . Jaim e, P . Lin, M B . Salam on, and P D . H an, Phys. Rev. B 58, R5901 (1998).
 - ⁹ P R . Broussard, S B . Q adri, V M . Browning, and V C . Cestone, J. Appl. Phys. 85, 6563 (1999).
 - ¹⁰ L . J . van der Pauw, Phillips Res. Rep. 13, 1 (1958).
 - ¹¹ Q . H uang, A . Santoro, J W . Lynn, R W . Erwin, J A . Borchers, J L . Peng, K . G hosh, and R L . G reene, Phys. Rev. B 58, 2684 (1998).
 - ¹² P . Schi er, A P . Ram irez, W . Bao, and S . W . Cheong, Phys. Rev. Lett. 75, 3336 (1995).
 - ¹³ V M . Browning, R M . Stroud, W W . Fuller-M ora, J M . Byers, M S . O sofsky, D L . Knies, K S . G rabowski, D . K oller, J . K in, D B . Chrisey, and J S . Horwitz, J. Appl. Phys. 83, 7070 (1998).
 - ¹⁴ X . W ang and X . G . Zhang, Phys. Rev. Lett. 82, 4276 (1999).
 - ¹⁵ J A . Nekker and R . M ead, Computer Journal 7, 308 (1965).
 - ¹⁶ J W . Lynn et al., Phys. Rev. Lett. 76, 4046 (1996).
 - ¹⁷ J A . Fernandez-Baca, P . Dai, H . Y . Hwang, C . K loc, and S W . Cheong, Phys. Rev. Lett. 80, 4012 (1998).
 - ¹⁸ G J . Snyder, R . H iskes, S . D iCarolis, M R . Beasley, and T H . G eballe, Phys. Rev. B . 53, 14434 (1996).

TABLE I: Results from fitting Eq.2 for the as grown films on NdGaO₃

x	ρ_0 (m Ω)	T_q (K)	ρ_2 (m Ω /K ²)	ρ_5 (m Ω /K ⁵)
0.333	0.271	31.7	27.1	1.99
0.247	0.498	26.5	49.7	2.61
0.218	0.625	26.2	64.4	3.44
0.20	0.323	21.3	37.7	1.64
0.184	0.375	23.5	40.7	2.11
0.122	0.506	9.9	49.7	3.4
0.097	0.477	14.4	45.9	2.82

TABLE II: Results from fitting Eq.2 for the as grown films on SrTiO₃

x	ρ_0 (m Ω)	T_q (K)	ρ_2 (m Ω /K ²)	ρ_5 (m Ω /K ⁵)
0.333	0.373	27.5	41.9	6.61
0.245	0.666	24.6	78.7	5.56
0.218	0.763	19.7	88.9	6.7
0.20	0.862	16.8	104	7.96
0.184	0.574	12.9	71.2	5.26

FIG .1: X-ray di raction scans along the Γ normal for LCMO Γ ($x=0.18$) grown on SrTiO₃ (dashed) and NdGaO₃ (solid) substrates.

FIG .2: X-ray di raction phi scans (a) along the LMO (022) (top) and NdGaO₃ (022) lines for LMO Γ ($x=0$) grown on NdGaO₃ and (b) along the LCMO (022) and SrTiO₃ (111) for a LCMO Γ ($x=1/3$) grown on SrTiO₃. The curves are offset for clarity.

FIG .4: Peak resistance temperature vs. polaronic activation energy for as grown and annealed LCMO Γ s on NdGaO₃ (NGO) and SrTiO₃ (STO). The Γ s labeled LCMO are from other samples of LCMO grown on a variety of substrates and di erent growth conditions by the author. The lines are guides to the eye.

FIG .5: Low temperature resistivity vs. temperature for the $x=0.18$ and 0.33 samples on NdGaO₃ and SrTiO₃ substrates along with the Γ s derived from Eq. 2

FIG .6: Low temperature resistivity vs. temperature for the $x=0.2$ sample on NdGaO₃ along with the Γ s derived from Eq. 2, Eq. 1 and the Mercone et al.⁷ model

FIG .7: Values of ρ_2 vs ρ_0 for the Γ s in this work, LSMO/LCMO composite Γ s,⁹ Pb-doped LCMO crystals,⁸ and LCMO thin Γ s¹⁸. The line is a guide to the eye.

FIG .3: Resistivity vs. temperature for as deposited La_{1-x}Ca_xMnO₃ Γ s on a) (100) NdGaO₃, and b) (001) SrTiO₃ for various values of x .

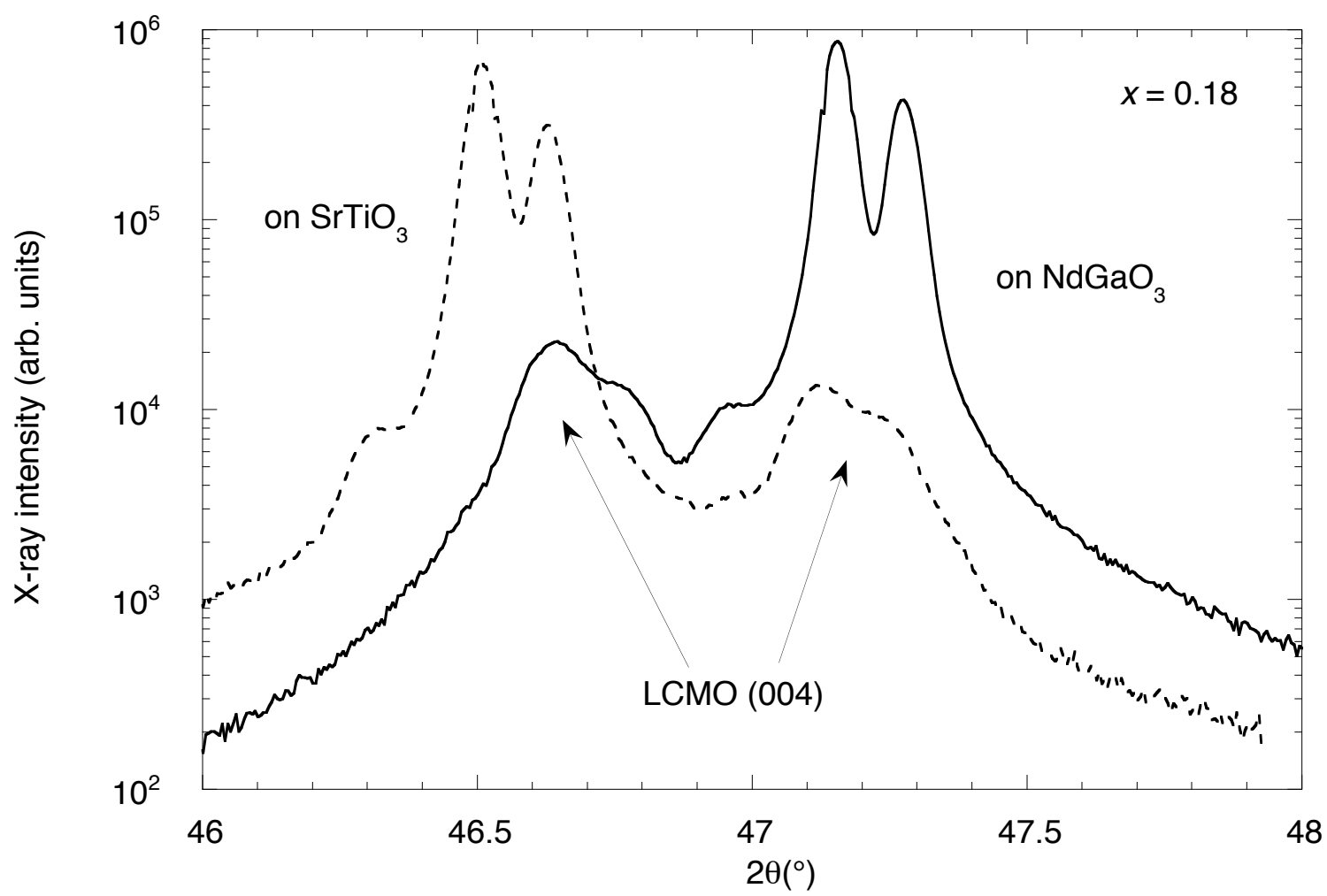


Figure 1

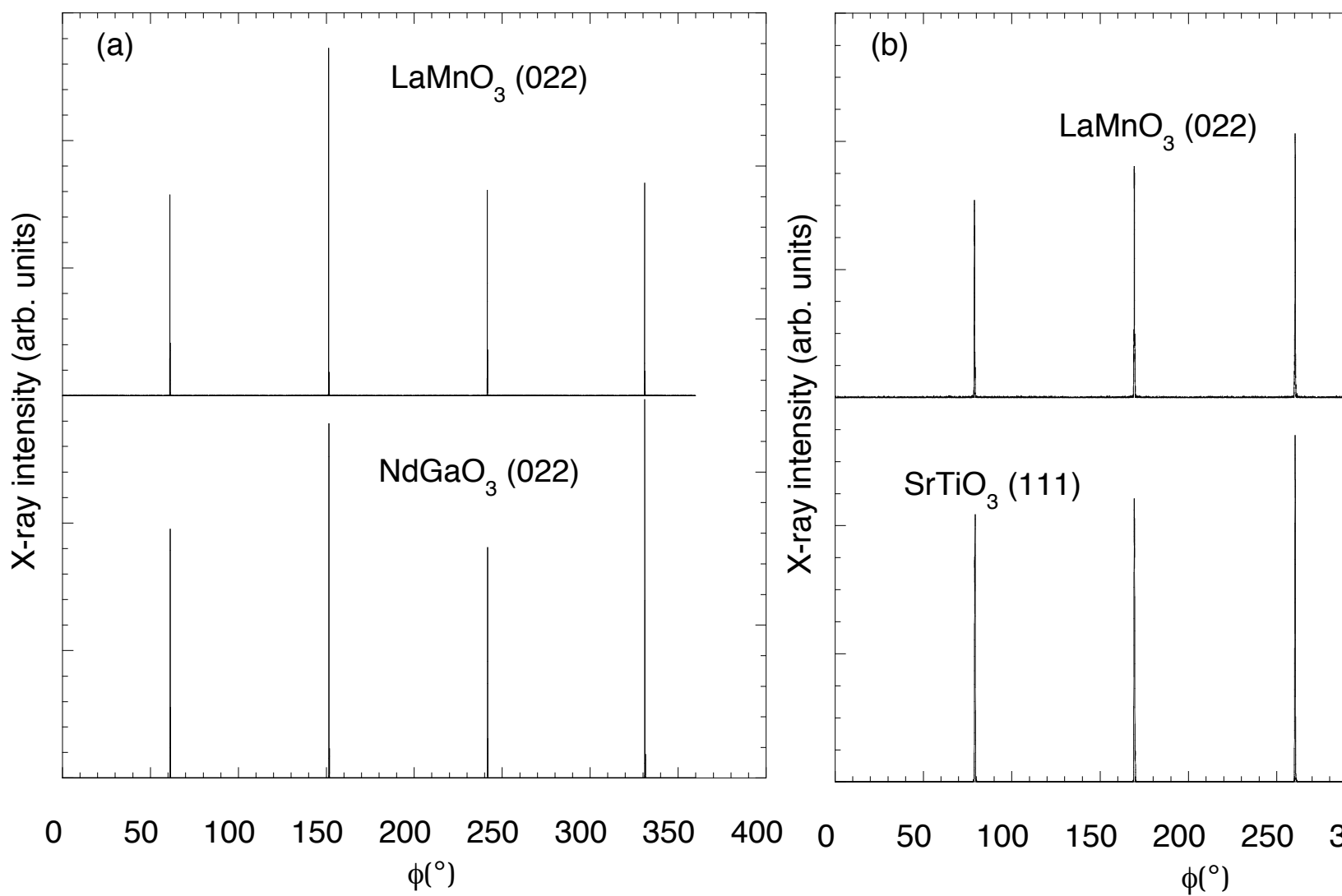


Figure 2

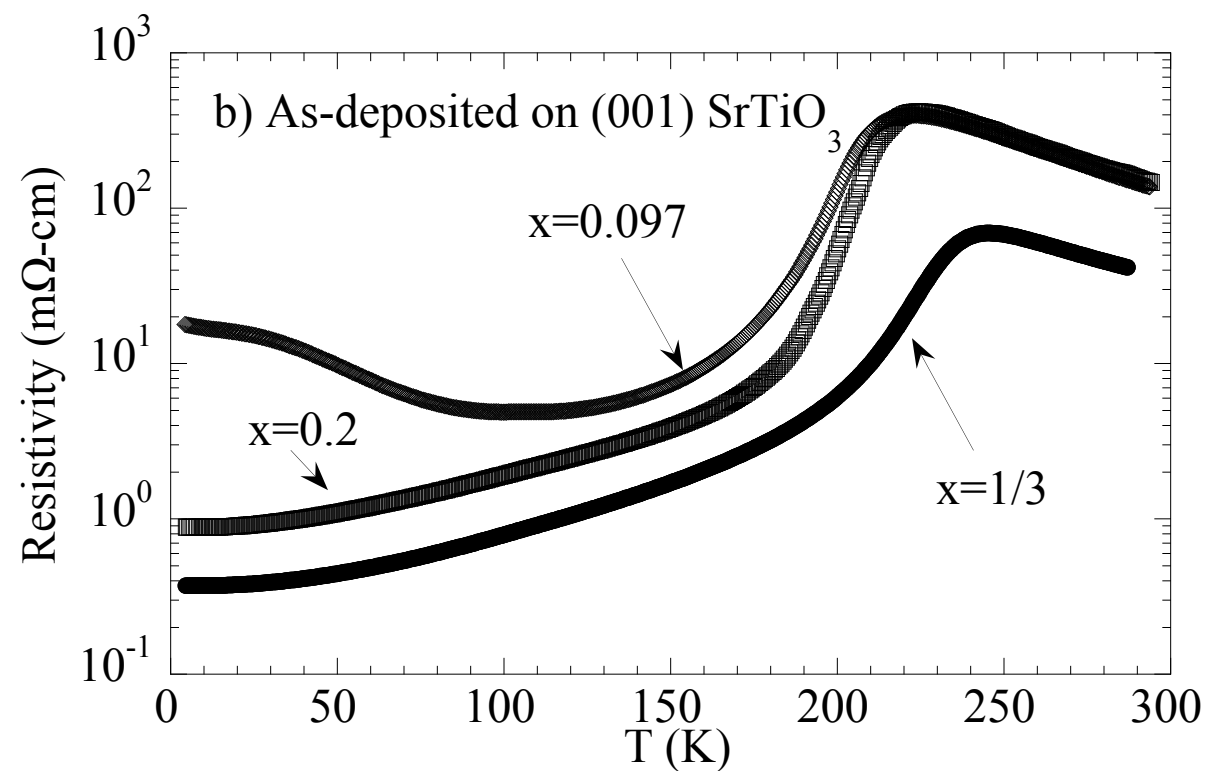
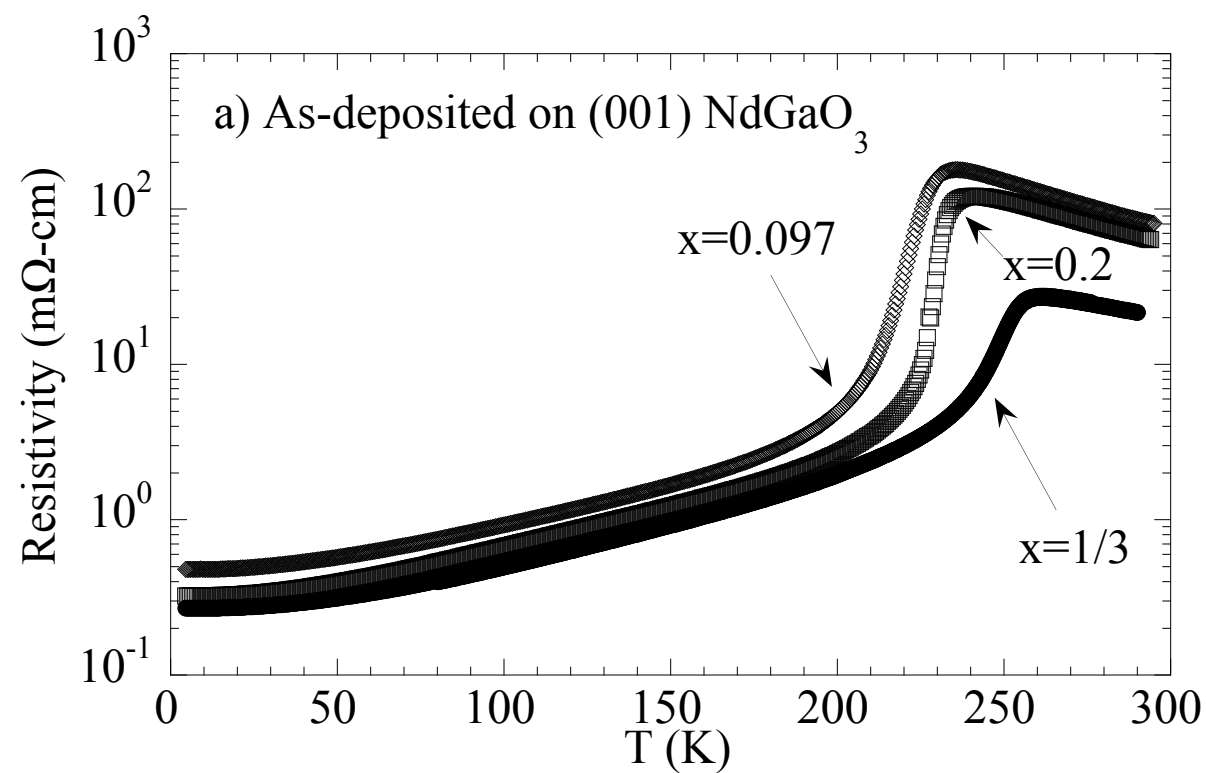


Figure 3

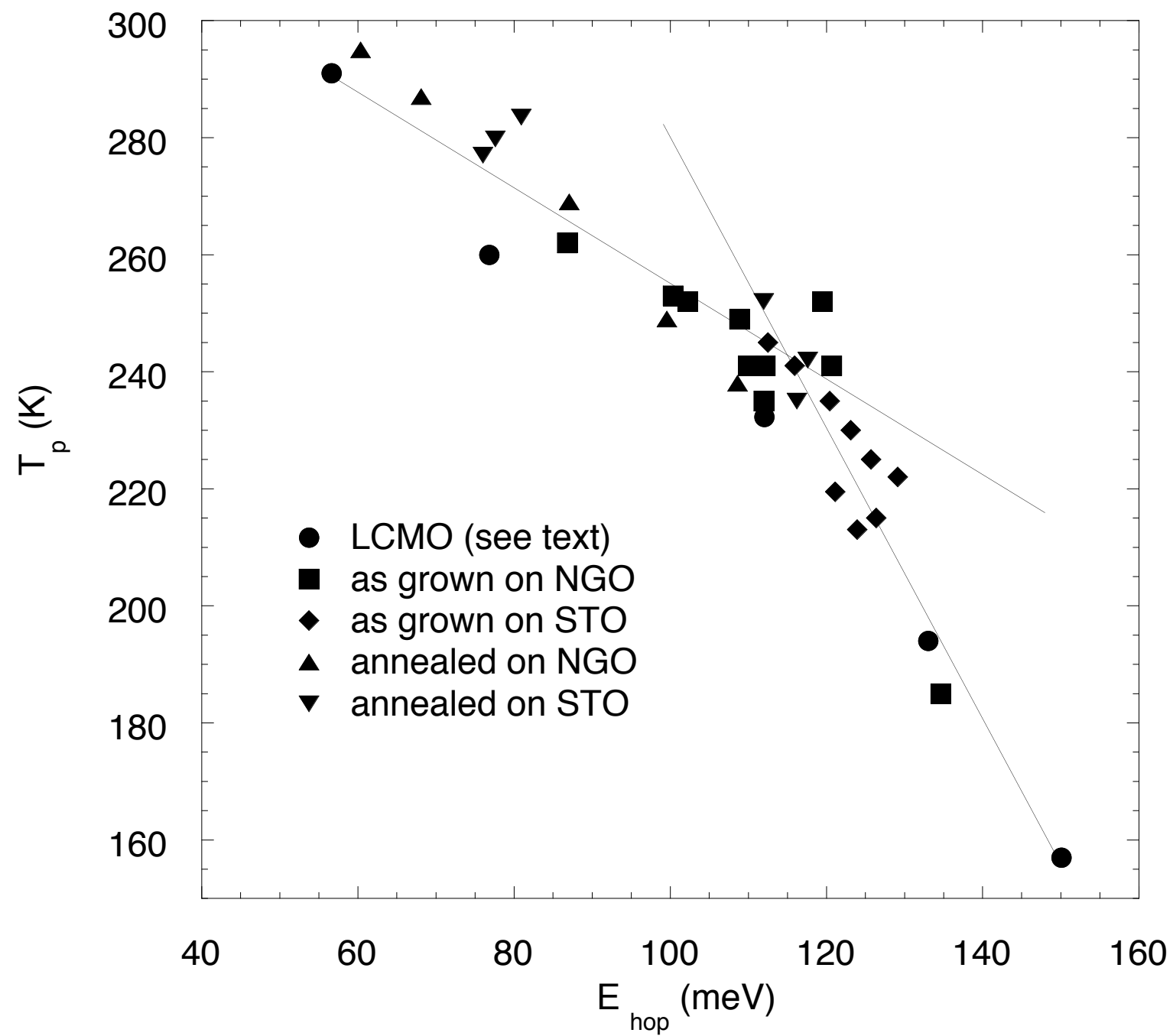


Figure 4

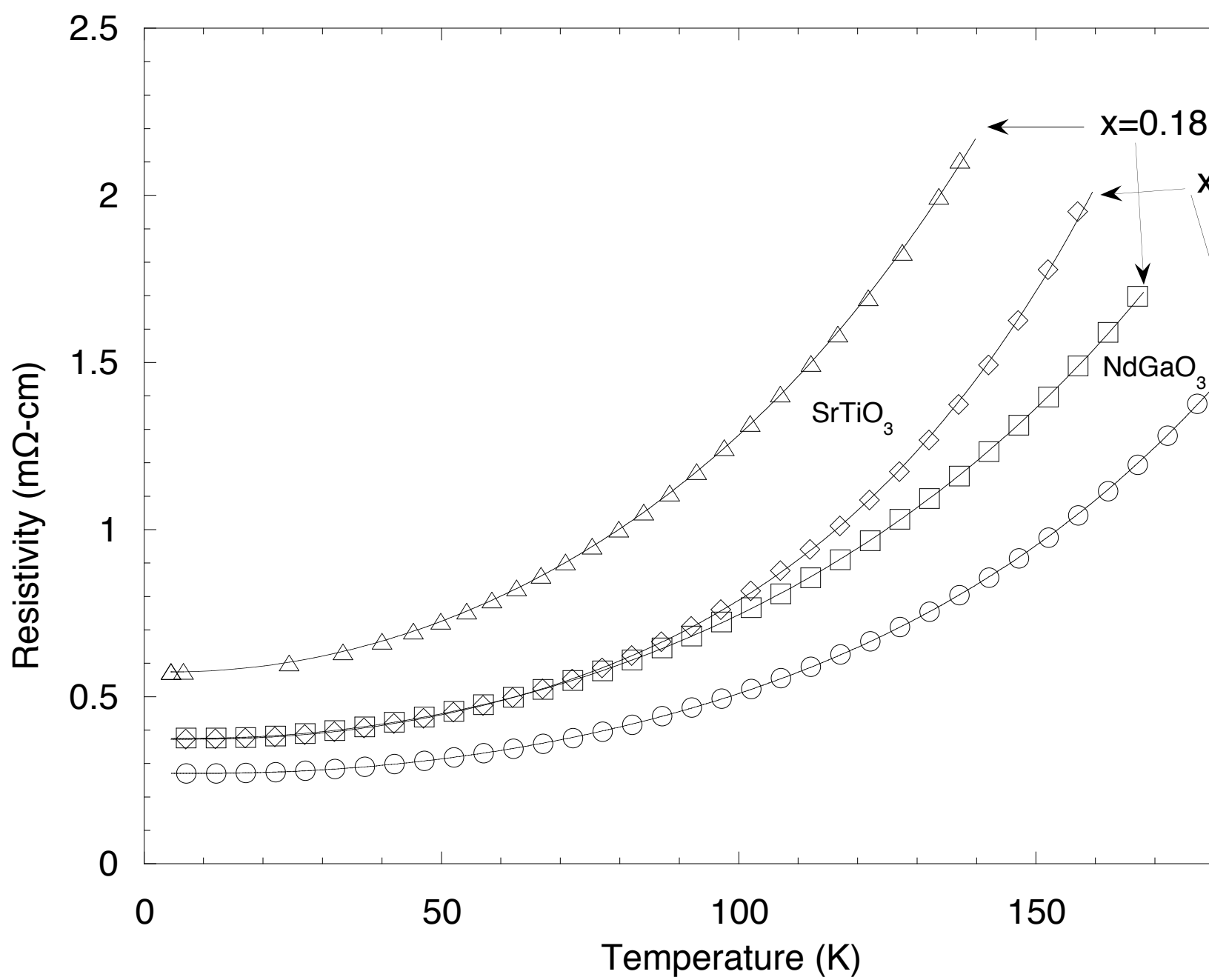


Figure 5

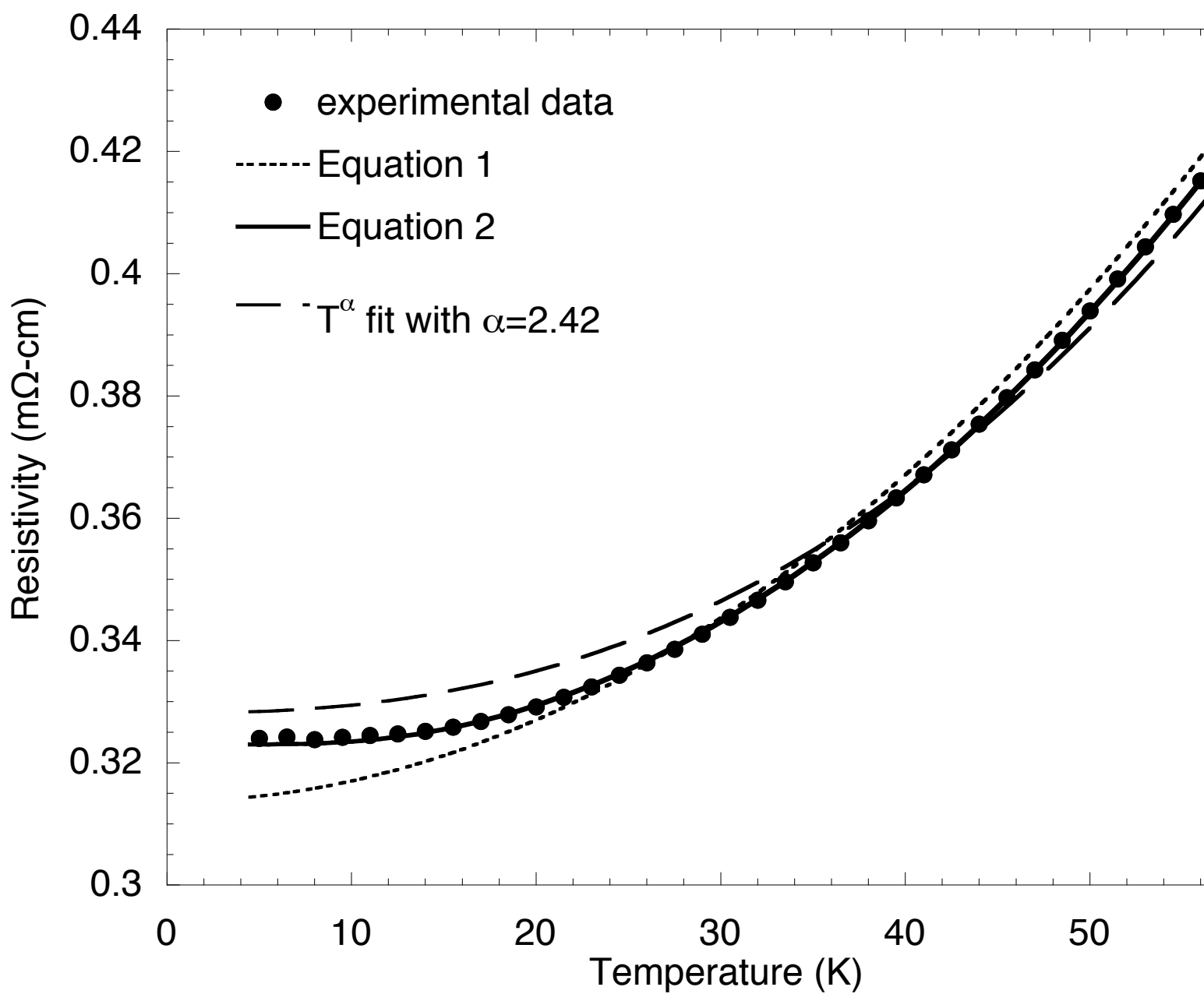


Figure 6

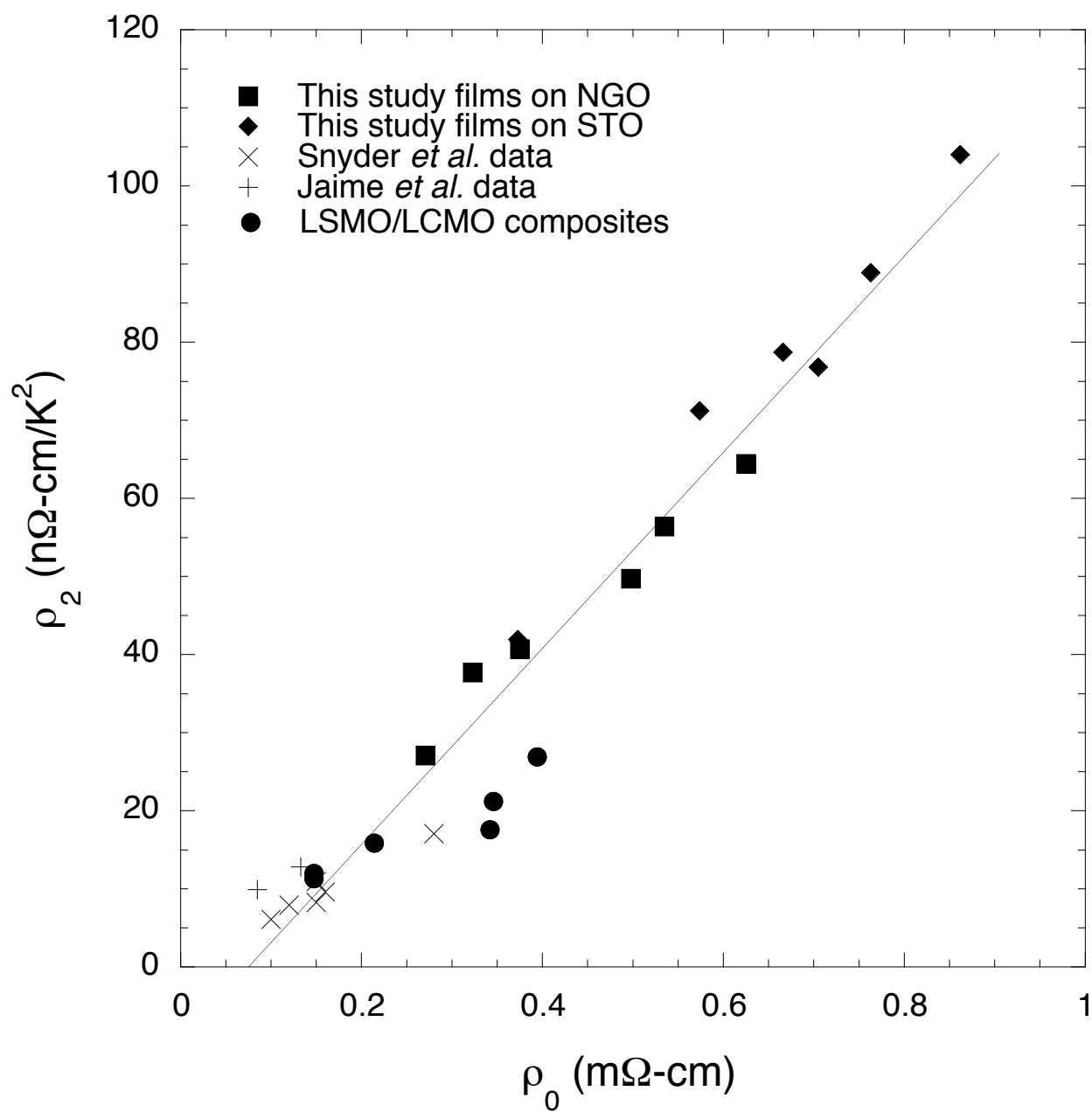


Figure 7